ISSN 0006-2979, Biochemistry (Moscow), 2019, Vol. 84, Suppl. 1, pp. S144-S158. © Pleiades Publishing, Ltd., 2019.
Russian Text © A. Yu. Sdobnov, J. Lademann, M. E. Darvin, V. V. Tuchin, 2019, published in Uspekhi Biologicheskoi Khimii, 2019, Vol. 59, pp. 295-322.

REVIEW

Methods for Optical Skin Clearing in Molecular Optical Imaging in Dermatology

A. Yu. Sdobnov[1,2,a]*, J. Lademann[3], M. E. Darvin[3#], and V. V. Tuchin[2,4,5,6#]

[1]*Faculty of Information Technology and Electrical Engineering, University of Oulu, 90570 Oulu, Finland*
[2]*Research-Educational Institute of Optics and Biophotonics, Saratov State University, 410012 Saratov, Russia*
[3]*Center of Experimental and Applied Cutaneous Physiology, Department of Dermatology, Venerology and Allergology, Charité – Universitätsmedizin Berlin, corporate member of Freie Universität Berlin, Humboldt-Universität zu Berlin, and Berlin Institute of Health, 10117 Berlin, Germany*
[4]*Laboratory of Laser Diagnostics of Technical and Living Systems, Institute of Precision Mechanics and Control, Russian Academy of Sciences, 410028 Saratov, Russia*
[5]*Interdisciplinary Laboratory of Biophotonics, Tomsk State University, 634050 Tomsk, Russia*
[6]*Bach Institute of Biochemistry, Research Center of Biotechnology of the Russian Academy of Sciences, 119071 Moscow, Russia*
[a]*e-mail: sdobnovanton@mail.ru*

Received August 15, 2018
Revised August 15, 2018
Accepted August 15, 2018

Abstract—This short review describes recent progress in using optical clearing (OC) technique in skin studies. Optical clearing is an efficient tool for enhancing the probing depth and data quality in multiphoton microscopy and Raman spectroscopy. Here, we discuss the main mechanisms of OC, its safety, advantages, and limitations. The data on the OC effect on the skin water content are presented. It was demonstrated that 70% glycerol and 100% Omnipaque™ 300 reduce the water content in the skin. Both OC agents (OCAs) significantly affect the strongly bound and weakly bound water. However, Omnipaque™ 300 causes considerably less skin dehydration than glycerol. In addition, the results of examination of the OC effect on autofluorescence in two-photon excitation and background fluorescence in Raman scattering at different skin depths are presented. It is shown that Omnipaque™ 300 is a promising OCA due to its ability to reduce background fluorescence in the upper skin layers. The possibility of multimodal imaging combining optical methods and OC technique is discussed.

DOI: 10.1134/S0006297919140098

Keywords: multiphoton microscopy, Raman spectroscopy, Raman microscopy, tissue, skin, optical clearing, dehydration

The skin is an outer organ that covers a body of vertebrates and forms a barrier between the organism and its environment [1, 2]. In addition to protecting the body from external factors and preventing pathogen penetration, the skin participates in thermal regulation, respiration, exchange processes, and regulation of water evaporation [3-5]. The skin is the largest organ of the human body with respect to its surface area. The investigation of its structure, early detection of skin diseases development, monitoring and control of medicinal drug penetration, and identification of age-related changes are important topics of modern biomedicine that can be successfully studied by molecular spectroscopy and imaging. As a rule, dermatologists initially perform visual skin examination, while skin biopsy is required for accurate diagnosis of oncological diseases. Since biopsy is an invasive and rather painful procedure that involves minor surgery, the development of noninvasive techniques for diagnostics of skin diseases, as well as methods for monitoring the penetration and action of medicinal drugs on various skin structures are important areas of modern scientific research.

Abbreviations: AF, autofluorescence; CARS, coherent anti-Stokes Raman spectroscopy; DMSO, dimethyl sulfoxide; MPT, multiphoton tomography; OC, optical clearing; OCA, optical clearing agent; OCT, optical coherence tomography; PA, photoacoustics; PAT, PA tomography; PEG, polyethylene glycol; RS, Raman spectroscopy; RM, Raman microscopy; SERS, surface enhanced Raman scattering; SHG, second harmonic generation.

* To whom correspondence should be addressed.
# These authors contributed equally to this work.

At present, there is a wide spectrum of noninvasive optical methods available for skin examination *in vivo*, such as optical coherence tomography (OCT) [6, 7], Raman spectroscopy (RS) [8-12], multiphoton tomography (MPT) [13-16], laser speckle visualization [17, 18], fluorescence spectroscopy [19, 20], laser scanning microscopy [21-23], and others. All these methods can be used for imaging. But the most promising approach in clinical studies is a combined use of several optical methods – the so-called multimodal imaging [24]. Combining several optical methods for examination of biological tissues allows to obtain information both at functional and molecular levels, thus enhancing the efficiency of diagnostics and the following control of the disease treatment. Numerous multimodal methods for skin visualization exist, such as combined use of OCT and photoacoustic tomography (PAT) [25], as well as of OCT and MPT [26]. Combination of terahertz (THz) pulse irradiation and polarization imaging was used for identifying cells in nonmelanoma skin cancer [27]. Confocal reflectometry was used in combination with autofluorescence tomography for detecting early stages of skin cancer [28]. It must be noted that skin examination by MPT often uses a combination of independent detection channels, e.g., autofluorescence (with excitation at different wavelengths), autofluorescence lifetime, second harmonic generation, and coherent anti-Stokes Raman scattering of lipids and water, which makes such examination multimodal [29-33]. As a rule, the use of multimodal optical methods in dermatology aims at increasing the detection limit in the diagnostics of various types of skin cancer.

However, all above-mentioned optical methods for skin examination have one critical limitation that prevents obtaining the information from the deep skin layers in the visible and infrared spectral regions. This limitation is associated with the fact that the stratum corneum and the living epidermis display especially high light scattering. Moreover, deeper skin layers, such as dermis and hypodermis, also have high scattering coefficients that are 10- and 100-fold higher, respectively, than their absorption coefficients [34, 35]. The method of optical clearing (OC) was developed in the 1990s in order to increase the probing depth of optical systems, as well as the spatial resolution and the contrast of the generated images [34, 36-38]. The effects of various optical clearing agents (OCAs), such as glycerol [39], glucose [40, 41], dimethyl sulfoxide (DMSO) [42], etc. on the skin and other biological tissue have been investigated using such optical methods as OCT [43, 44], MPT [45, 46], RS [47, 48], PAT [49-54], photoacoustic flow cytometry (PAFC) [55], and others.

In this review we present the results of RS and MPT studies on the efficiency of OC in optical molecular imaging used for diagnostics of skin diseases. The possibility of combined application of RS, MPT, and X-ray computed tomography for multimodal imaging of pathological tissues is discussed.

MAJOR MECHANISMS OF OPTICAL CLEARING

The scattering anisotropy (g) and scattering coefficient (μ_s) of biological tissues are determined by the difference of the refractive indices (n) of the interstitial fluid and cell components (nuclei, organelles, membranes, and cytoplasm) and/or scleroprotein fibrous structures of the dermis, muscle, and cartilage [56]. At present, refractive indices in the visible and infrared spectral ranges are known for a number of main components of biological tissues, such as nuclei and cytoplasmic organelles in mammalian cells [57], oxygenated and deoxygenated hemoglobin [58, 59], collagen in connective tissues [60], and others.

In this work, we will limit ourselves to discussing the immersion OC, when the matching of the refractive indices in a tissue is achieved via tissue immersion in an OCA. Currently, three main hypothetical mechanisms of OC are considered by the scientific community [61]. The first mechanism explains the matching of the refractive indices of different components of biological tissues and tissue liquids by OCA penetration into the tissues [34, 36, 41, 43, 61-66]. The second mechanism is associated with a dehydration of biological tissues caused by the hyperosmolar properties of OCAs [34, 37, 41, 62, 66-68]. The third mechanism is related to the OCA effect on reversible dissociation of collagen fibers in the dermis [66, 69-72], i.e., destabilization of collagen structure via OCA interference with the hydrogen bonds formed by collagen molecules resulting in the decrease of light scattering by collagen structures due to the decrease in the size of scattering particles [67, 73]. It is important to note that the three described mechanisms of OCA action do not occur independently, but rather in interaction. Moreover, the relative contribution of each mechanism depends on the type of biological tissue, the molecular structure of OCA, its concentration, and so on. It was suggested in a number of publications that dehydration caused by an OCA could decrease the scattering in soft tissues by displacing water from the space between the collagen fibers, thus decreasing the difference between the refractive indices of tissue components [34, 44, 74, 75]. For example, the refractive index of water at 589 nm is 1.33, while the refractive index of human epidermis at the same wavelength is 1.44, of dermis – 1.39, and of 70% glycerol aqueous solution and 100% Omnipaque^{TM} 300 – 1.43 [46, 76, 77]. A significant decrease in the refractive index after OC has been demonstrated in a number of studies [36, 75, 78-81]. Moreover, structural changes caused by the dehydration include compression of biological tissues and, as a result, an increase in their transparency due to the interference phenomena occurring upon light scattering by the ordered structures.

Hence, the OC efficiency in biological tissues can depend on numerous factors, such as OCA refractive index, osmolarity, concentration, etc., as well as on the original turbidity of biological tissue and its permeability

for a particular OCA. Selecting an OCA with the optimal parameters is a complex and important issue. If this problem is solved, deep layers of biological tissues could be investigated efficiently and noninvasively. One also must consider that the OC efficiency in *in vivo* studies also depends on such physiological features of the tissue as the metabolic response to OCA, temperature, and tissue functional properties (blood supply, availability of developed lymphatic system) [34, 37, 61, 65, 67, 79, 82-85]. Furthermore, the refractive indices of living tissue components depend on tissue physiological and pathological state. It should be also considered that glycerol and glucose injections directly into the skin affect microhemocirculation in the dermis, and the extent of this effect depends on the OCA concentration and duration of its action [49, 86, 87].

OPTICAL CLEARING AGENTS AND ENHANCERS

Since the beginning of OC application, a large number of compounds and their combinations have been tested, with some of them demonstrating high efficiencies in the imaging of biological tissues. All the known OCAs for the application by immersion can be arbitrarily divided into the following groups: (i) polyatomic alcohols [glycerol, polyethylene glycol (PEG), polypropylene glycol] and solutions of sorbitol, polypropylene glycol, PEG, xylitol, glycerol, and mannitol [44, 68, 78-80, 82, 86-95]; (ii) sugars (glucose, fructose, ribose, sucrose, and dextrose) [41, 70, 71, 84-87, 96-99]; (iii) organic acids (oleic and linoleic acids) [50, 100]; (iv) other organic solvents, such as DMSO [39, 50, 66, 100, 101] or thiazone [102-108]; (v) radiocontrast agents (Verografin™, Trasograph™, Hypaque™, and Omnipaque™) [46, 48]. Presently the most popular OCAs, especially for skin clearing, are glycerol, glucose, and PEG due to their good biocompatibility and pharmacokinetics in biological tissues [43, 45, 62, 105, 109-111]. Although these OCAs are considered as nontoxic, prolonged exposure of living tissues to these agents can result in negative effects, such as local hemostasis, extreme tissue compression, and in some cases, even necrosis (if OCA is injected into the skin). It was demonstrated that glycerol-mediated dissociation of collagen fibers could cause morphological changes in the dermis and tendons in rodents [71, 72]. Moreover, glycerol affects skin blood vessels, in particular, causes venous and arterial stasis [112]. It was also demonstrated that the application of glucose or glycerol could result in the temporary blockage of blood flow in the surface vessels [86, 87]. It was mentioned in a number of publications that some OCAs could cause edema and irritation in tissues [68, 79, 81, 84, 85].

Hence, one of the most important problems in safe *in vivo* imaging of living tissues is the selection of an optimal OCA, its concentration, and exposure time. Recent studies demonstrated that iohexol (5-[acetyl(2,3-dihydroxypropyl)amino]-N,N′-bis(2,3-dihydroxypropyl)-2,4,6-triiodobenzene-1,3-dicarboxamide) manufactured under the trade name Omnipaque™ is a promising OCA for *in vivo* studies. Solutions with iohexol concentrations of 300 mg/ml (Omnipaque™ 300) [48, 113, 114] and 350 mg/ml (Omnipaque™ 350) [44], respectively, were successfully used as OCAs for an efficient imaging of deep layers of biological tissues. The low osmolarity of this compound (465 mOsm/liter) allows avoiding deformation of skin layers. Furthermore, in comparison with glycerol, Omnipaque™ causes a significantly milder skin dehydration [46, 48].

As was mentioned above, the efficiency of OC depends on many factors. Among them are the type of OCA, its concentration, as well as the time of biological tissue exposure to the agent. For example, in some cases, tissue clearing to complete transparency takes several weeks [64]. Considering that the skin barrier function, provided by the stratum corneum, prevents the penetration of high OCA concentrations to the deep layers of the dermis, OC of the skin requires more time compared to other types of biological tissues. Considering that low OCA concentrations cannot ensure a sufficient efficiency of OC and prolonged exposure to highly concentrated OCAs could negatively affect the skin, methods allowing one to accelerate the process of OC have been introduced.

Ethanol, propylene glycol, DMSO, linoleic and oleic acids are commonly used as chemical enhancers to accelerate the penetration of OCAs [39, 61, 66, 97, 101, 103, 104, 106-108, 111, 115-121]. Moreover, DMSO, propylene, and oleic acid by themselves are often used as OCAs [39, 50, 66, 91, 122-125]. Skin pretreatment with ethanol allows to modify the properties of the stratum corneum, as well as to accelerate the OCA penetration via skin appendages and directly through the epidermis [95, 120]. In addition, ethanol removes oil from the skin surface, which also accelerates OC.

In addition to the use of chemical enhancers, biological tissues are often subjected to physical treatment immediately before the OCA application. The most popular among the physical methods are removal of the stratum corneum surface layers with an adhesive tape (tape stripping) [126], microdamage of epidermis [127], microdermabrasion [128], photothermal and mechanical perforation [129], laser irradiation of skin surface [130, 131], electrophoresis [132], treatment with ultrasound [133], and others.

MULTIPHOTON TOMOGRAPHY

Multiphoton tomography (MPT) is an efficient tool for noninvasive *in vivo* skin examination [134]. Based on two- and three-photon excitation of fluorophores, this

method allows one to investigate the 3D distribution of fluorophores in thick biological samples. In general, this type of imaging is possible because fluorophore excitation in the ultraviolet range, for example, at 380 nm, is realized via irradiation of the investigated tissue with femtosecond laser pulses at a wavelength of 760 nm. Considering that biological tissues are highly transparent at this wavelength, MPT allows one to generate images of deep skin layers (up to the depth of ~200 μm). The autofluorescence signal of skin induced by two-photon excitation (further referred to as autofluorescence, AF) is related to the fluorescence of NAD(P)H, elastin, melanin, and to a lesser degree, keratin. The second harmonic generation signal (SHG) is emitted by collagen type I molecules. As a rule, the wavelengths longer than the wavelengths of AF and SHG are used in MPT for signal excitation. The main drawback of MPT lies in the fact that strong scattering in biological tissues critically decreases the penetration depth of the focused laser radiation to the depth that is even smaller than for the equivalent one-photon fluorescence microscopy [135]. That is why the application of OCAs in MPT studies of biological objects can significantly enhance the potential of this nonlinear optical imaging method.

The results of investigation of one of the OC mechanisms were reported in [72]. The authors proposed the molecular mechanism of OC based on the fact that the saturation of rodent dermis and tail tendon with anhydrous (100%) glycerol resulted in the temporal and reversible loss of collagen fiber organization in these tissues. Such type of changes in the collagen structure, as well as a decrease in the diameter of collagen fibers, could result in the decrease of scattering.

The possibility to increase the depth of imaging in the two-photon tomography (TPT) using OCAs was first described by Cicchi et al. in [45]. In this study, human dermis was exposed to hyperosmotic agents (glucose, glycerol, and polypropylene glycol) for several minutes. It was found that glycerol was the most efficient OCA (relative contrast was 16.3 at a depth of 20 μm), but at the same time, the slowest. Propylene glycol solution was the second best in its efficiency as an OCA (relative contrast was 12.6 at a depth of 20 μm). Glucose action was the least efficient OCA with the relative contrast of 5.1 at a depth of 20 μm. However, OC with glucose was 3 times faster than with glycerol.

It was shown in [135] that a combination of confocal microscopy and TPT followed by 3D imaging could be used for noninvasive examination of the collagen structure. In this study, the authors used a mixture of DMSO, diatrizoic acid, and glucamine as an OCA. The described mixture is widely known as FocusClear and was patented in 2002 [136]. Compared to pure DMSO and glycerol, FocusClear provided a significantly better transmittance at 488, 543, and 633 nm and brighter fluorescence at 505 nm [135]. Moreover, the combined use of TPP and fluorescence microscopy made it possible to assign unique morphological and spectroscopic characteristics to different components of human skin [137]. The most important is the fact that the produced data allowed to distinguish between healthy skin and tissues affected by melanoma and basal cell carcinoma. The possibility of diagnostics of squamous cell carcinoma and preceding actinic keratosis based on the epidermis morphological parameters determined *in vivo* using MPT without OC was demonstrated in [138].

MPT was used to establish the course of events occurring during glycerol action on tissues containing collagen structures [139]. The first stage was fast tissue dehydration accompanied by a compression of the collagen network. Then, the process of relatively slow penetration of OCA into the collagen interfibrillar space took place. It was also found that the low-concentration glycerol solution produced a significantly reduced OC effect, presumably due to the fact that in the course of OC, water molecules in the tissue are partially replaced with glycerol molecules. The greater the number of glycerol molecules, the more effective the OC. The authors also demonstrated that the effects caused by the application of 100% glycerol or phosphate buffer mixed with glycerol (50/50%) for several minutes were reversible.

The use of glycerol as an OCA resulted in the decrease in the diffuse reflection coefficient of rat skin *in vivo* [68]. Moreover, skin treatment with 75% glycerol solution for 30 min cleared the skin to transparency. This process was also accompanied by a decrease of the dermis thickness from 1459 to 1287 μm and decrease in the diameter of collagen fibers from 109 to 79 nm due to the displacement of water from the tissue by glycerol. However, collagen fibers were not dissolved or fractured. In this connection, the authors suggested that one of the most important mechanisms of OC is associated with the changes in the thickness of the tissue layer (its compression) resulting in the emergence of a more dense and regular packing of tissue fibers and decrease in the fiber diameter due to the dehydration of the interfibrillar matter and collagen fibers themselves.

It is important to note that the reduction of scattering due to OC significantly increases the fluorescence yield until the clearing window reaches the emitting fluorophores. Considering that in the absence of scattering, the path of the excitation photon decreases, the probability that this photon will encounter the fluorophore and excite it also decreases. Nevertheless, if this excitation takes place, the emitted photon has a high probability of reaching the detector due to low scattering. Hence, one must consider that a strong OC would result in the loss of signal [140].

In order to evaluate the possibility of using OC *in vivo*, we studied the OC efficiency in porcine skin following a short-term application of biologically compatible agents, such as glycerol and Omnipaque™ 300

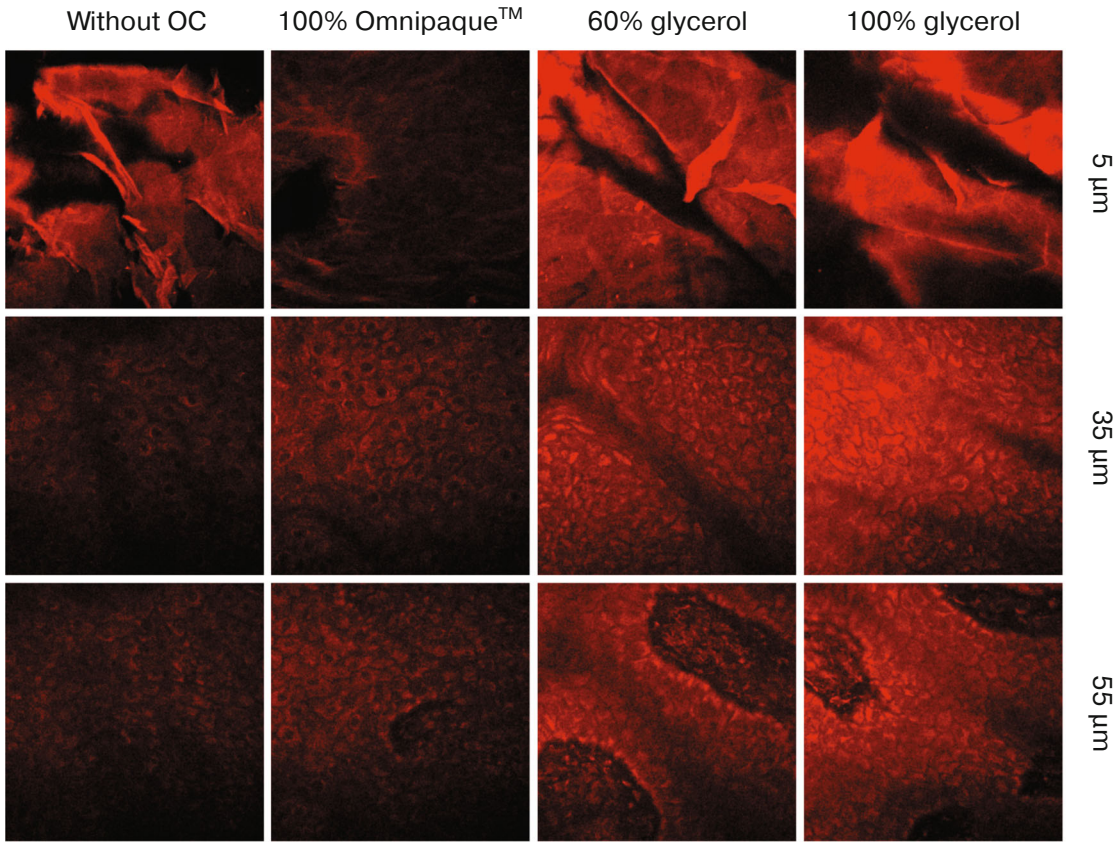

Fig. 1. Autofluorescence images of the untreated porcine skin and skin treated with 60 and 100% glycerol solutions and 100% Omnipaque™ 300 generated at different depths *ex vivo*. Excitation wavelength, 760 nm.

(iohexol) [46]. It was shown that with both OCAs, skin treatment for 1 h (i.e., time interval suitable for *in vivo* applications) significantly increased the imaging depth and the contrast of AF and SHG images. Figure 1 shows AF images at different depths for the control skin sample and samples treated with 60 and 100% glycerol solutions and 100% Omnipaque™ 300. By comparing the effects of OC obtained with 40, 60, and 100% glycerol solutions and 60 an 100% Omnipaque™ 300 solutions, we found that the SHG signal intensity was affected less by 100% glycerol solution than by 40 and 60% glycerol solutions, which could be associated with a high viscosity of the highly concentrated glycerol solution that prevented its penetration into the skin. In addition, a higher degree of tissue dehydration in this case could also be the reason for a lower SHG efficiency. Despite the fact that both glycerol and Omnipaque™ 300 provided significant OC, glycerol was more efficient as an OCA, although it caused a pronounced compression of skin tissues and changes in cell morphology. No such effects were observed for Omnipaque™ 300 solution, and that is why we suggest it as a safe and fast-acting OCA for clinical tests.

RAMAN SPECTROSCOPY

The detection of inelastically scattered light in the process of vibrational and rotational energy exchange between the probing radiation and molecules of the irradiated sample constitutes the basis of Raman spectroscopy (RS). The Raman spectrum of a biological tissue can be considered as a tissue molecular fingerprint containing information on its chemical composition. Any small changes in cells and tissues can result in pronounced changes in the Raman spectrum. Hence, RS represents a proper technology for elucidating the chemical composition of various types of biological tissues [141-143]. RS and Raman microscopy (RM) are commonly used in dermatology for *in vivo* analysis of the epidermis (mostly, stratum corneum) [144-147]. In addition, RS is actively used for monitoring the penetration of xenobiotics through the skin [148-150]. However, due to the strong light scattering by skin, RS has strict limitations in the *in vivo* applications (the probing depth, as a rule, is limited by the thickness of the epidermis, i.e., ~40-50 μm). Because OC is accompanied by a decrease in the elastic light scattering, this allows to achieve a more

efficient interaction of the probing laser beam with the investigated tissue. Hence, the use of OC in combination with RS provides a significant improvement in clinical testing.

Enejder et al. [151] used RS for quantitative noninvasive (transcutaneous) evaluation of glucose levels in the blood of healthy volunteers, whose blood glucose levels were elevated using a standard peroral glucose tolerance test protocol. For the sake of simplicity in the presentation and comparison of the results, the authors used the spectral range of 400 to 2000 cm^{-1} with the excitation at 785 nm (the emergence of the Raman signal in this wavenumber region results from different vibrations in molecules). In the majority of cases, the Raman peaks correspond to particular molecular vibrations or types of molecules, which provides the information on the biochemical composition of the studied biological tissue [152, 153]. The possibility to monitor OCA penetration and distribution in human skin was demonstrated in [117] using unique properties of the Raman spectrum of DMSO. It was established that the major portion of the DMSO solution penetrated stratum corneum within 20 min.

An important finding was that OCAs could increase the signal-to-noise ratio, significantly enhance the Raman signal, and decrease the systematic error emerging due to an inaccurate determination of the surface and sub-surface spectra [152].

A multimodal approach combining MPT (SHG imaging, in particular) and CARS (coherent anti-Stokes Raman scattering spectroscopy) for investigating the OC effect of DMSO in human skin was described in [154]. The authors suggested that DMSO interacts with collagen fibers and changes the distance between the fibers at a sub-micron scale. It was shown that the skin scattering decreased when 40% aqueous DMSO solution was used, but not the DMSO solution with lower (20%) concentration. Hence, this work provided an important validation for the fact that the mechanisms underlying the correlation between the refractive indices of tissue components and structural changes of collagen fibers play an important role in OC. In addition, it was demonstrated that the DMSO concentration changed with time at the different skin depths, which allowed one to determine the diffusion coefficient of DMSO in the skin. The maximum DMSO concentration decreased from 40 to 10% at a depth of 25 μm (epidermis) within 3 h. This decrease was accompanied by skin dehydration and reduction of the stratum corneum barrier function. This study demonstrated that CARS could be an efficient technique for quantitative analysis of OC.

The OC of porcine skin after local application of 40, 60, and 80% glycerol aqueous solutions for 0 to 75 min was studied in [155]. The authors demonstrated that the use of glycerol allowed one to increase significantly the registration depth of the Raman spectra. It was also shown that the increase in the glycerol concentration from 40 to 80% resulted in a more efficient OC.

Kim et al. demonstrated that the Raman spectrum of porcine skin depends on the skin water content. In particular, the ratio of protein peaks at 1450 and 1660 cm^{-1} differed significantly for the skin samples with a water content of 40, 45, 50, and 55% [156]. This fact was confirmed by the process modeling using the Monte-Carlo method. An increase in the water content affects to a greater extent the distribution of the backscattering in the larger angular region rather than increasing its intensity. Hence, the authors suggested that the skin water content should be controlled during the measurements in order to provide an accurate diagnostics of skin diseases by RS. A detailed comparative analysis of the water distribution in the stratum corneum depending on the strength of hydrogen bonds was conducted in [157] for porcine skin *ex vivo* and human skin *in vivo*.

Considering that the Raman signal strongly depends on the presence of elastic scattering [158, 159], the fact that highly concentrated OCAs could decrease scattering to such a degree that the Raman signal would be lost must be taken into account. Therefore, a compromise must be sought in the OC-facilitated measurements between the increase in the Raman signal upon strong scattering and the loss of Raman signal in the absence of scattering [158, 160]. Hence, in order to measure Raman in living tissues, it is important to find a biocompatible OCA and to optimize its concentration so that the Raman signal from a pre-set depth is at its maximum

Considering that strong scattering in biological tissues and weak intensity of Raman signal result in the decreased resolution and contrast of the Raman spectra, methods based on the Surface Enhanced Raman Scattering (SERS) have attracted considerable attention, since they allow one to significantly increase the sensitivity of Raman measurements in the skin [161-165]. The possibility of further increasing the SERS sensitivity was demonstrated in murine skin studies using a number of OCAs [166], out of which FPT (a mixture of fructose, PEG-400, and thiazone) demonstrated the highest efficiency. The maximum effect was recorded 15 min after FPT application and was 3.5-fold higher than the effect of fructose solution.

A method for *in vivo* determination of the composition of various types of tattoo ink based on the analysis of Raman spectra was suggested in a recent study by Darvin et al. [167]. The use of glycerol allowed one to increase the depth of probing from 50 to 400 μm.

Recently, we have investigated the effects of 70% glycerol and 100% Omnipaque™ 300 solutions on porcine skin 30 and 60 min after their application [48]. Figure 2 shows the representative Raman spectra of the control skin samples and samples treated with glycerol solution and Omnipaque™ 300 recorded in a wavenumber range of 400-2000 cm^{-1} at different depths. The

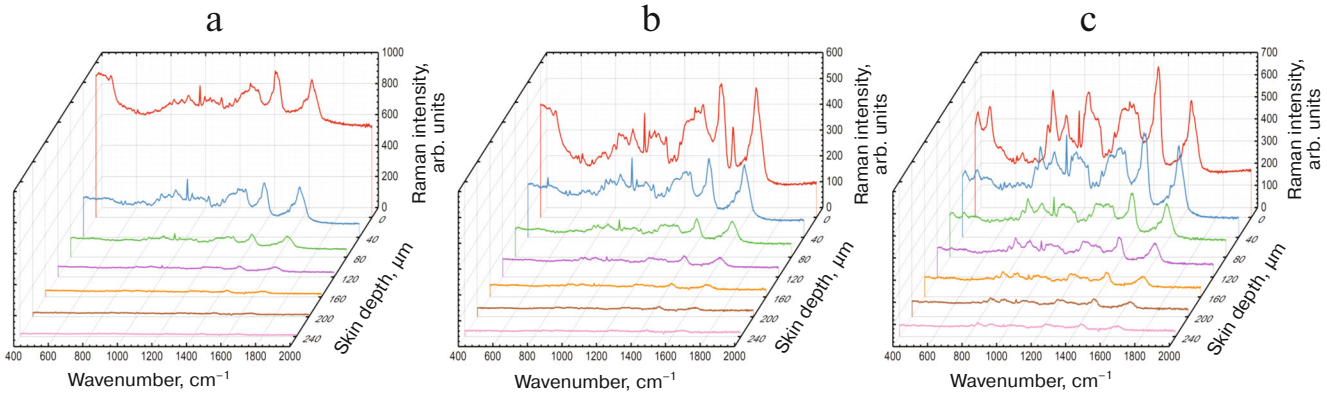

Fig. 2. Raman spectra of porcine skin recorded *ex vivo* at different depths: a) control sample; b) sample treated with 100% Omnipaque™300 solution for 1 h; c) sample treated with 70% glycerol solution for 1 h. Excitation wavelength, 785 nm.

intensity of the Raman peaks corresponding to the skin molecular components increased significantly at the depths below 160 μm following 60-min treatment with Omnipaque™ 300. In the case of glycerol, an increased peak intensity was observed starting at the depth of 40 μm. We also investigated the OCA effect on the collagen hydration in the dermis. It was established that both OCAs caused skin dehydration, but the effect of Omnipaque™ 300 was significantly less pronounced. To better understand the action of OCAs on the skin water content, we analyzed the Raman spectra in the wavenumber range of 2000-4000 cm^{-1}. The convolution procedure was conducted for each Raman spectrum using 10 Gaussian functions as described in detail in [168]. Next, four Gaussian function were selected peaking at 3005, 3277, 3458, and 3604 cm^{-1} in order to analyze the water composition with respect to the strength of hydrogen bonds. These peaks corresponded to four types of skin water: 3005 cm^{-1} – tightly bound water (DAA-OH: one donor, two acceptors); 3277 cm^{-1} – strongly bound water (DDAA-OH: two donors, two acceptors); 3458 cm^{-1} – weakly bound water (DA-OH: one donor, one acceptor); 3604 cm^{-1} – unbound water (superposition of very weakly bound water DDA-OH: two donors, one acceptor and free water). Next, the surface area under the curve was calculated for each of the Gaussian functions. The obtained values were normalized with respect to the surface area under the curve for the Gaussian function with the peak at 2930 cm^{-1} (proteins [169]). The results of our calculations for the samples treated with 70% glycerol and 100% Omnipaque™ 300 solution for 30 and 60 min are presented in Fig. 3 together with the control data (untreated skin).

It can be seen in Fig. 3a that the fraction of tightly bound water reduced following the treatment with both clearing agents, although glycerol has a more profound effect than Omnipaque™ 300. Omnipaque™ 300 caused a significant decrease in the fraction of strongly bound water only after 60-min treatment at a depth of 80-200 μm (Fig. 3b). Glycerol, on the other hand, produced a strong effect starting at a depth of 40 μm (Fig. 3b). The treatment with Omnipaque™ 300 for 30 and 60 min increased the peaks corresponding to strongly bound and weakly bound water at a depth of 40 μm. Similar effect was observed for the unbound water following 60-min treatment with Omnipaque™ 300 (detailed results of this study are reported in our recent publication [170]). Considering that Omnipaque™ 300 penetrates to the depths of 35-40 μm within 1 h, this increase can be associated with the fact that water contained in Omnipaque™ 300 supplements water in the skin. Another explanation could be that normalization to the protein peak is not entirely correct for the depth of 40 μm, because this depth corresponds to the spinous layer that has less protein that the stratum corneum and the dermis [171]. It can be seen in Fig. 3c that both OCAs affected similarly the weakly bound and strongly bound water. Application of glycerol decreased the content of unbound water starting from the depth of 40 μm. (Fig. 3d). The effect of Omnipaque™ 300 became pronounced only after 1-h treatment starting from the depth of 80 μm. Both OCAs exhibited the largest effect on the strongly bound and weakly bound water. These results demonstrate that glycerol caused a higher degree of skin dehydration than Omnipaque™ 300. This conclusion is in agreement with our previous studies [48] and confirms once again that Omnipaque™ 300 offers many promises as an OCA agent for clinical tests. Furthermore, it can be used for quantitative evaluation of the OCA effect on individual skin components (e.g., collagen). And finally, Omnipaque™ 300 can be applied to monitor the liquid flows caused by OCA application.

We also used MPT to investigate the effect of OCAs on the porcine skin fluorescence [46]. The data produced by RM and MPT are presented for comparison in Figs. 4a and 4b, respectively. For RM, fluorescence was calculated as an integral value of background fluorescence; AF signal was used in MPT.

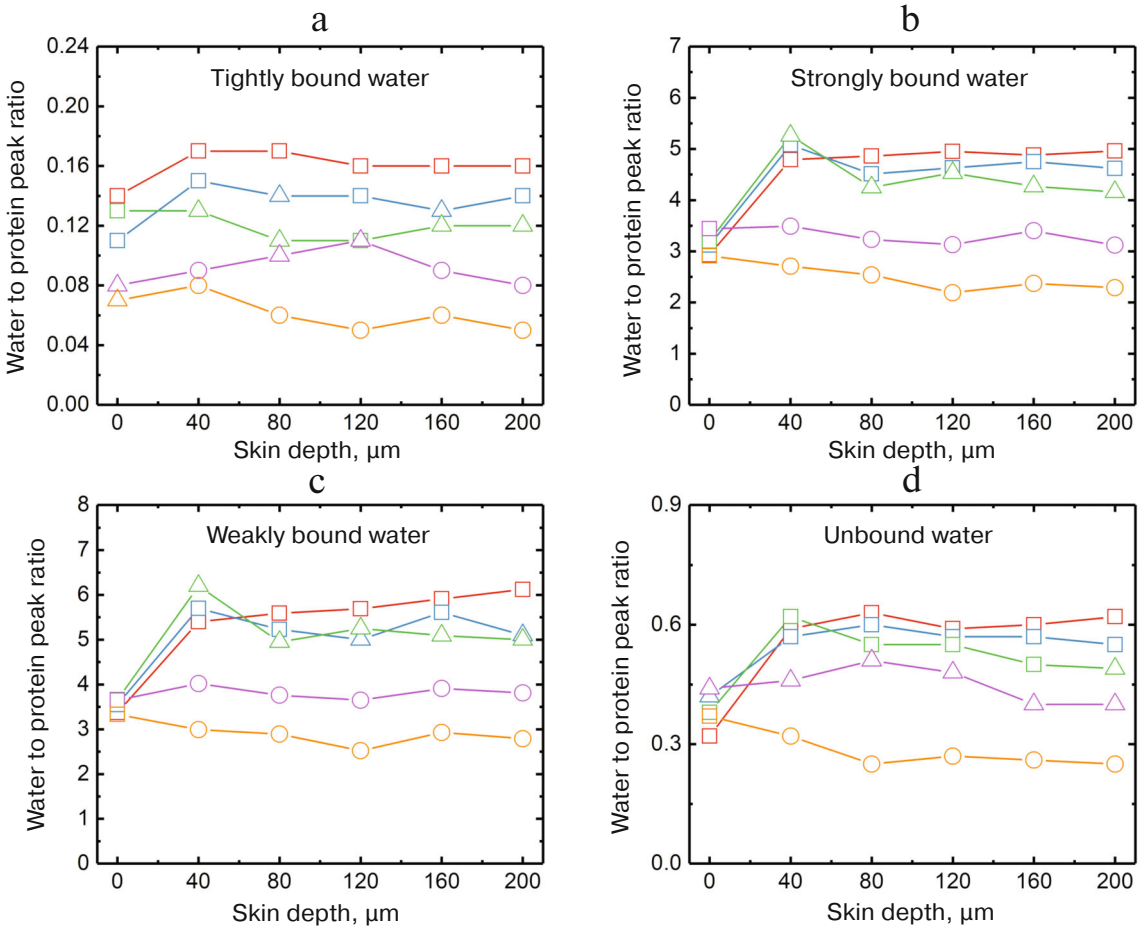

Fig. 3. Peak values for (a) tightly bound water, (b) strongly bound water, (c) weakly bound water, and (d) unbound water normalized to protein peak for different depths of porcine skin *ex vivo*. Red, without OC; blue, 30-min application of Omnipaque™ 300; green, 60-min application of Omnipaque™ 300; purple, 30-min application of glycerol; orange, 60-min application of glycerol. Mean values are presented; squares, statistically insignificant difference between the control and OCA-treated samples, $p > 0.05$; triangles, statistically significant difference between the control and OCA-treated samples, $p < 0.05$; circles, statistically significant difference between the control and OCA-treated samples, $p < 0.01$.

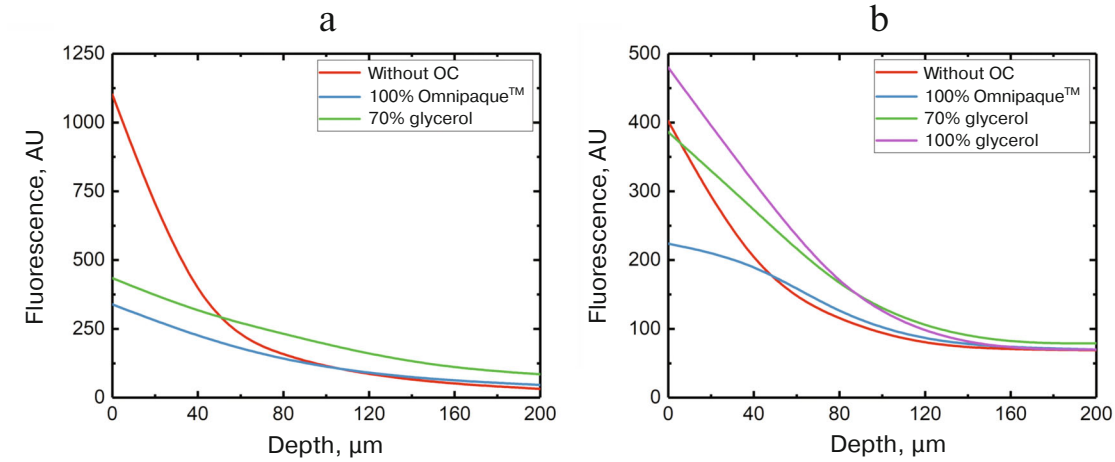

Fig. 4. a) Background fluorescence of the Raman spectra (excitation wavelength, 785 nm) for the control skin samples and samples treated with 70% glycerol solution and 100% Omnipaque™ 300. b) MPT fluorescence (excitation wavelength, 760 nm) for control skin samples and samples treated with 70 and 100% glycerol solutions and 100% Omnipaque™ 300.

The application of both OCAs resulted in a significant decrease of background fluorescence at the depths up to 50 μm due to OCA immersion (Fig. 4a). At larger depths, the background fluorescence in the samples treated with Omnipaque™ 300 was comparable to the fluorescence of control samples, while the use of glycerol caused an increase in the background fluorescence. This effect of glycerol is associated with the fact that more excitation light reached deeply located fluorophores due to the decrease of scattering; the fluorescence signal is additionally enhanced due to less scattering. Omnipaque™ 300 also caused a significant decrease in the AF signal at the depths up to 50 μm due to OCA immersion (Fig. 4b); at the depths of 50-160, this signal was slightly higher than in the control samples. At the depths exceeding 160 μm, the AF signal was similar in the control and Omnipaque™ 300-treated samples. It is important to note that skin treatment with the 60% glycerol solution resulted in the increase of the AF signal, which was contrary to the control samples at all depths except the skin surface. The use of 100% glycerol also caused an increase of the AF signal from the depths up to 160 μm. This effect of glycerol can be most likely explained by the decrease of scattering due to the strong skin dehydration.

Hence, the produced data prove that Omnipaque™ 300 is an exceptionally efficient OCA. Besides causing significantly less dehydration than glycerol, it is more efficient in decreasing the background fluorescence in the upper skin layers, which is an interfering factor in RM. Moreover, since Omnipaque™ 300 is a radiocontrast agent, it could potentially be used in the multimodal studies combining optical methods and micro-X-ray skin imaging.

Optical clearing is an efficient technique for controlling the optical properties of biological objects that allows one to increase the probing depth and to improve the quality of the obtained information. The search for new safe and efficient OCAs and elucidation of the mechanisms of their action in biological tissues are important research areas. In this work, we briefly reviewed the results of studies on the use of optical clearing to improve the quality of optical diagnostics in dermatology, with emphasis on RM and MPT of skin. The results of studies on the effect of glycerol and Omnipaque™ 300 on the tightly bound, strongly bound, weakly bound, and unbound water were presented. In particular, it was shown that both OCAs affected mostly the strongly bound and weakly bound water. Glycerol demonstrated a significantly higher dehydration effect than Omnipaque™ 300. We also studied the effect of these OCAs on fluorescence in RM and MPT. Based on the available data, Omnipaque™ 300 is an exceptionally efficient OCA that significantly decreases the background fluorescence in the upper skin layers.

There is a large number of optical methods available for studying biological tissues at the molecular level in addition to RS and MPT that are less efficient in the case of strong scattering. Moreover, many biological tissues still remain poorly understood with respect to optical clearing, especially under *in vivo* conditions. This opens new prospects for further multimodal studies and the development of novel techniques for the imaging of biological tissues and an analysis of their parameters using controlled optical clearing.

Funding

This work was financially supported by the Government of the Russian Federation, grant no. 14.W03.31.0023.

REFERENCES

1. Agache, P., and Humbert, P. (2004) *Measuring the Skin*, Springer Science Business Media, Berlin.
2. Potts, R. (1997) Skin barrier: principles of percutaneous absorption, *Arch. Dermatol.*, **133**, 924-924.
3. Yokota, M., and Tokudome, Y. (2016) The effect of glycation on epidermal lipid content, its metabolism and change in barrier function, *Skin Pharmacol. Physiol.*, **29**, 231-242.
4. Proksch, E., Brandner, J. M., and Jensen, J. M. (2008) The skin: an indispensable barrier, *Exp. Dermatol.*, **17**, 1063-1072.
5. Van Smeden, J., Janssens, M., Kaye, E. C., Caspers, P. J., Lavrijsen, A. P., Vreeken, R. J., and Bouwstra, J. A. (2014) The importance of free fatty acid chain length for the skin barrier function in atopic eczema patients, *Exp. Dermatol.*, **23**, 45-52.
6. Fercher, A. F. (1996) Optical coherence tomography, *J. Biomed. Opt.*, **1**, 157-173.
7. Gambichler, T., Pljakic, A., and Schmitz, L. (2015) Recent advances in clinical application of optical coherence tomography of human skin, *Clin. Cosmet. Invest. Dermatol.*, **8**, 345-354.
8. Darvin, M. E., Gersonde, I., Albrecht, H., Gonchukov, S. A., Sterry, W., and Lademann, J. (2005) Determination of beta carotene and lycopene concentrations in human skin using resonance Raman spectroscopy, *Laser Phys.*, **15**, 295-299.
9. Vyumvuhore, R., Tfayli, A., Piot, O., Le Guillou, M., Guichard, N., Manfait, M., and Baillet-Guffroy, A. (2014) Raman spectroscopy: *in vivo* quick response code of skin physiological status, *J. Biomed. Opt.*, **19**, 111603.
10. Krafft, C., and Popp, J. (2015) The many facets of Raman spectroscopy for biomedical analysis, *Anal. Bioanal. Chem.*, **407**, 699-717.
11. Choe, C., Lademann, J., and Darvin, M. E. (2016) A depth-dependent profile of the lipid conformation and lateral packing order of the stratum corneum *in vivo* measured using Raman microscopy, *Analyst*, **141**, 1981-1987.
12. Darvin, M. E., Sterry, W., Lademann, J., and Vergou, T. (2011) The role of carotenoids in human skin, *Molecules*, **16**, 10491-10506.

13. Konig, K., and Riemann, I. (2003) High-resolution multiphoton tomography of human skin with subcellular spatial resolution and picosecond time resolution, *J. Biomed. Opt.*, **8**, 432-439.
14. Balu, M., Mikami, H., Hou, J., Potma, E. O., and Tromberg, B. J. (2016) Rapid mesoscale multiphoton microscopy of human skin, *Biomed. Opt. Express*, **7**, 4375-4387.
15. Shirshin, E. A., Gurfinkel, Y. I., Priezzhev, A. V., Fadeev, V. V., Lademann, J., and Darvin, M. E. (2017) Two-photon autofluorescence lifetime imaging of human skin papillary dermis *in vivo*: assessment of blood capillaries and structural proteins localization, *Sci. Rep.*, **7**, 1171.
16. Shirshin, E. A., Gurfinkel, Y. I., Matskeplishvili, S. T., Sasonko, M. L., Omelyanenko, N. P., Yakimov, B. P., Lademann, J., and Darvin, M. E. (2018) *In vivo* optical imaging of the viable epidermis around the nailfold capillaries for the assessment of heart failure severity in humans, *J. Biophotonics*, **11**, e201800066.
17. Abookasis, D., and Moshe, T. (2014) Feasibility study of hidden flow imaging based on laser speckle technique using multiperspectives contrast images, *Opt. Laser Eng.*, **62**, 38-45.
18. Sdobnov, A., Bykov, A., Molodij, G., Kalchenko, V., Jarvinen, T., Popov, A., Kordas, K., and Meglinski, I. (2018) Speckle dynamics under ergodicity breaking, *J. Phys. D. Appl. Phys.*, **51**, 155401.
19. Ferulova, I., Lihachev, A., and Spigulis, J. (2015) Photobleaching effects on *in vivo* skin autofluorescence lifetime, *J. Biomed. Opt.*, **20**, 051031.
20. Maciel, V. H., Correr, W. R., Kurachi, C., Bagnato, V. S., and da Silva Souza, C. (2017) Fluorescence spectroscopy as a tool to *in vivo* discrimination of distinctive skin disorders, *Photodiagn. Photodyn. Ther.*, **19**, 45-50.
21. Lademann, J., Patzelt, A., Darvin, M., Richter, H., Antoniou, C., Sterry, W., and Koch, S. (2008) Application of optical non-invasive methods in skin physiology, *Laser Phys. Lett.*, **5**, 335-346.
22. Ulrich, M., Klemp, M., Darvin, M. E., Konig, K., Lademann, J., and Meinke, M. C. (2013) *In vivo* detection of basal cell carcinoma: comparison of a reflectance confocal microscope and a multiphoton tomograph, *J. Biomed. Opt.*, **18**, 61229.
23. Darvin, M. E., Richter, H., Meinke, M. C., Knorr, F., Lademann, J., Zhu, Y. J., Gonchukov, S. A., and Koenig, K. (2014) Comparison of *in vivo* and *ex vivo* laser scanning microscopy and muliphoton tomography application for human and porcine skin imaging, *Quantum Electron.*, **44**, 646-651.
24. Marti-Bonmati, L., Sopena, R., Bartumeus, P., and Sopena, P. (2010) Multimodality imaging techniques, *Contrast Media Mol. Imaging*, **5**, 180-189.
25. Chen, Z., Rank, E., Meiburger, K. M., Sinz, C., Hodul, A., Zhang, E., Hoover, E., Minneman, M., Ensher, J., Beard, P. C., Kittler, H., Leitgeb, R. A., Drexler, W., and Liu, M. Y. (2017) Non-invasive multimodal optical coherence and photoacoustic tomography for human skin imaging, *Sci. Rep.*, **7**, 17975.
26. Konig, K., Speicher, M., Buckle, R., Reckfort, J., McKenzie, G., Welzel, J., Koehler, M. J., Elsner, P., and Kaatz, M. (2009) Clinical optical coherence tomography combined with multiphoton tomography of patients with skin diseases, *J. Biophotonics*, **2**, 389-397.
27. Fan, B., Neel, V. A., and Yaroslavsky, A. N. (2017) Multimodal imaging for nonmelanoma skin cancer margin delineation, *Laser Surg. Med.*, **49**, 319-326.
28. Peng, T., Xie, H., Ding, Y. C., Wang, W. C., Li, Z. M., Jin, D. Y., Tang, Y. H., Ren, Q. S., and Xi, P. (2012) CRAFT: multimodality confocal skin imaging for early cancer diagnosis, *J. Biophotonics*, **5**, 469-476.
29. Konig, K., Raphael, A. P., Lin, L., Grice, J. E., Soyer, H. P., Breunig, H. G., Roberts, M. S., and Prow, T. W. (2011) Applications of multiphoton tomographs and femtosecond laser nanoprocessing microscopes in drug delivery research, *Adv. Drug Deliver Rev.*, **63**, 388-404.
30. Patalay, R., Talbot, C., Alexandrov, Y., Munro, I., Neil, M. A. A., Konig, K., French, P. M. W., Chu, A., Stamp, G. W., and Dunsby, C. (2011) Quantification of cellular autofluorescence of human skin using multiphoton tomography and fluorescence lifetime imaging in two spectral detection channels, *Biomed. Opt. Express*, **2**, 3295-3308.
31. Darvin, M. E., Konig, K., Kellner-Hoefer, M., Breunig, H. G., Werncke, W., Meinke, M. C., Patzelt, A., Sterry, W., and Lademann, J. (2012) Safety assessment by multiphoton fluorescence/second harmonic generation/hyper-rayleigh scattering tomography of ZnO nanoparticles used in cosmetic products, *Skin Pharmacol. Physiol.*, **25**, 219-226.
32. Sanchez, W. Y., Obispo, C., Ryan, E., Grice, J. E., and Roberts, M. S. (2013) Changes in the redox state and endogenous fluorescence of *in vivo* human skin due to intrinsic and photo-aging, measured by multiphoton tomography with fluorescence lifetime imaging, *J. Biomed. Opt.*, **18**, 061217.
33. Breunig, H. G., Weinigel, M., Buckle, R., Kellner-Hofer, M., Lademann, J., Darvin, M. E., Sterry, W., and Konig, K. (2013) Clinical coherent anti-Stokes Raman scattering and multiphoton tomography of human skin with a femtosecond laser and photonic crystal fiber, *Laser Phys. Lett.*, **10**, 025604.
34. Tuchin, V. V. (2015) *Tissue Optics: Light Scattering Methods and Instruments for Medical Diagnostics*, SPIE Press, Bellingham.
35. Gratton, E. (2011) Deeper tissue imaging with total detection, *Science*, **331**, 1016-1017.
36. Tuchin, V. V., Maksimova, I. L., Zimnyakov, D. A., Kon, I. L., Mavlyutov, A. H., and Mishin, A. A. (1997) Light propagation in tissues with controlled optical properties, *J. Biomed. Opt.*, **2**, 401-417.
37. Tuchin, V. V. (2006) *Optical Clearing of Tissues and Blood*, SPIE Press, Bellingham.
38. Sdobnov, A. Y., Darvin, M. E., Genina, E. A., Bashkatov, A. N., Lademann, J., and Tuchin, V. V. (2018) Recent progress in tissue optical clearing for spectroscopic application, *Spectrochim. Acta, A. Mol. Biomol. Spectrosc.*, **197**, 216-229.
39. Jiang, J., Boese, M., Turner, P., and Wang, R. K. (2008) Penetration kinetics of dimethyl sulphoxide and glycerol in dynamic optical clearing of porcine skin tissue *in vitro* studied by Fourier transform infrared spectroscopic imaging, *J. Biomed. Opt.*, **13**, 021105.
40. Larin, K. V., and Tuchin, V. V. (2008) Functional imaging and assessment of the glucose diffusion rate in epithelial tissues in optical coherence tomography, *Quantum Electron.*, **38**, 551-556.

41. Tuchina, D. K., Shi, R., Bashkatov, A. N., Genina, E. A., Zhu, D., Luo, Q., and Tuchin, V. V. (2015) *Ex vivo* optical measurements of glucose diffusion kinetics in native and diabetic mouse skin, *J. Biophotonics*, **8**, 332-346.
42. Bui, A. K., McClure, R. A., Chang, J., Stoianovici, C., Hirshburg, J., Yeh, A. T., and Choi, B. (2009) Revisiting optical clearing with dimethyl sulfoxide (DMSO), *Lasers Surg. Med.*, **41**, 142-148.
43. Tuchin, V. V., Xu, X. Q., and Wang, R. K. (2002) Dynamic optical coherence tomography in studies of optical clearing, sedimentation, and aggregation of immersed blood, *Appl. Optics*, **41**, 258-271.
44. Bykov, A., Hautala, T., Kinnunen, M., Popov, A., Karhula, S., Saarakkala, S., Nieminen, M. T., Tuchin, V., and Meglinski, I. (2016) Imaging of subchondral bone by optical coherence tomography upon optical clearing of articular cartilage, *J. Biophotonics*, **9**, 270-275.
45. Cicchi, R., Pavone, F. S., Massi, D., and Sampson, D. D. (2005) Contrast and depth enhancement in two-photon microscopy of human skin *ex vivo* by use of optical clearing agents, *Opt. Express*, **13**, 2337-2344.
46. Sdobnov, A., Darvin, M. E., Lademann, J., and Tuchin, V. (2017) A comparative study of *ex vivo* skin optical clearing using two-photon microscopy, *J. Biophotonics*, **10**, 1115-1123.
47. Schulmerich, M. V., Cole, J. H., Dooley, K. A., Morris, M. D., Kreider, J. M., and Goldstein, S. A. (2008) Optical clearing in transcutaneous Raman spectroscopy of murine cortical bone tissue, *J. Biomed. Opt.*, **13**, 021108.
48. Sdobnov, A. Y., Tuchin, V. V., Lademann, J., and Darvin, M. E. (2017) Confocal Raman microscopy supported by optical clearing treatment of the skin – influence on collagen hydration, *J. Phys. D. Appl. Phys.*, **50**, 285401.
49. Liopo, A., Su, R., Tsyboulski, D. A., and Oraevsky, A. A. (2016) Optical clearing of skin enhanced with hyaluronic acid for increased contrast of optoacoustic imaging, *J. Biomed. Opt.*, **21**, 081208.
50. Liu, Y. Y., Yang, X. Q., Zhu, D., Shi, R., and Luo, Q. M. (2013) Optical clearing agents improve photoacoustic imaging in the optical diffusive regime, *Opt. Lett.*, **38**, 4236-4239.
51. Zhao, Q. L., Li, L., Li, Q., Jiang, X., Ren, Q. S., Chai, X. Y., and Zhou, C. Q. (2014) Concentration dependence of optical clearing on the enhancement of laser-scanning optical-resolution photoacoustic microscopy imaging, *J. Biomed. Opt.*, **19**, 36019.
52. Zhou, Y., Yao, J. J., and Wang, L. H. V. (2013) Optical clearing-aided photoacoustic microscopy with enhanced resolution and imaging depth, *Opt. Lett.*, **38**, 2592-2595.
53. Yang, X. Q., Liu, Y. Y., Zhu, D., Shi, R., and Luo, Q. M. (2014) Dynamic monitoring of optical clearing of skin using photoacoustic microscopy and ultrasonography, *Opt. Express*, **22**, 1094-1104.
54. Yang, X. Q., Zhang, Y., Zhao, K., Zhao, Y. J., Liu, Y. Y., Gong, H., Luo, Q. M., and Zhu, D. (2016) Skull optical clearing solution for enhancing ultrasonic and photoacoustic imaging, *IEEE Trans. Med. Imaging*, **35**, 1903-1906.
55. Menyaev, Y. A., Nedosekin, D. A., Sarimollaoglu, M., Juratli, M. A., Galanzha, E. I., Tuchin, V. V., and Zharov, V. P. (2013) Optical clearing in photoacoustic flow cytometry, *Biomed. Opt. Express*, **4**, 3030-3041.
56. Tuchin, V. V., Wang, L., and Zimnyakov, D. A. (2006) *Optical Polarization in Biomedical Applications*, Springer Science and Business Media, Berlin.
57. Drezek, R., Dunn, A., and Richards-Kortum, R. (1999) Light scattering from cells: finite-difference time-domain simulations and goniometric measurements, *Appl. Optics*, **38**, 3651-3661.
58. Friebel, M., and Meinke, M. (2006) Model function to calculate the refractive index of native hemoglobin in the wavelength range of 250-1100 nm dependent on concentration, *Appl. Optics*, **45**, 2838-2842.
59. Lazareva, E. N., and Tuchin, V. V. (2018) Measurement of refractive index of hemoglobin in the visible/NIR spectral range, *J. Biomed. Opt.*, **23**, 1-9.
60. Leonard, D. W., and Meek, K. M. (1997) Refractive indices of the collagen fibrils and extrafibrillar material of the corneal stroma, *Biophys. J.*, **72**, 1382-1387.
61. Genina, E. A., Bashkatov, A. N., and Tuchin, V. V. (2010) Tissue optical immersion clearing, *Expert Rev. Med. Devices*, **7**, 825-842.
62. Larin, K. V., Ghosn, M. G., Bashkatov, A. N., Genina, E. A., Trunina, N. A., and Tuchin, V. V. (2012) Optical clearing for OCT image enhancement and in-depth monitoring of molecular diffusion, *IEEE J. Sel. Top. Quantum Electron.*, **18**, 1244-1259.
63. Hama, H., Hioki, H., Namiki, K., Hoshida, T., Kurokawa, H., Ishidate, F., Kaneko, T., Akagi, T., Saito, T., Saido, T., and Miyawaki, A. (2015) Sca/eS: an optical clearing palette for biological imaging, *Nat. Neurosci.*, **18**, 1518-1529.
64. Hama, H., Kurokawa, H., Kawano, H., Ando, R., Shimogori, T., Noda, H., Fukami, K., Sakaue-Sawano, A., and Miyawaki, A. (2011) Scale: a chemical approach for fluorescence imaging and reconstruction of transparent mouse brain, *Nat. Neurosci.*, **14**, 1481-1488.
65. Zhu, D., Larin, K. V., Luo, Q. M., and Tuchin, V. V. (2013) Recent progress in tissue optical clearing, *Laser Photonics Rev.*, **7**, 732-757.
66. Bui, A. K., McClure, R. A., Chang, J., Stoianovici, C., Hirshburg, J., Yeh, A. T., and Choi, B. (2009) Revisiting optical clearing with dimethyl sulfoxide (DMSO), *Laser Surg. Med.*, **41**, 142-148.
67. Tuchin, V. V. (2007) A clear vision for laser diagnostics (review), *IEEE J. Sel. Top. Quantum Electron.*, **13**, 1621-1628.
68. Wen, X., Mao, Z. Z., Han, Z. Z., Tuchin, V. V., and Zhu, D. (2010) *In vivo* skin optical clearing by glycerol solutions: mechanism, *J. Biophotonics*, **3**, 44-52.
69. Hirshburg, J., Choi, B., Nelson, J. S., and Yeh, A. T. (2006) Collagen solubility correlates with skin optical clearing, *J. Biomed. Opt.*, **11**, 040501.
70. Hirshburg, J., Choi, B., Nelson, J. S., and Yeh, A. T. (2007) Correlation between collagen solubility and skin optical clearing using sugars, *Laser Surg. Med.*, **39**, 140-144.
71. Hirshburg, J. M., Ravikumar, K. M., Hwang, W., and Yeh, A. T. (2010) Molecular basis for optical clearing of collagenous tissues, *J. Biomed. Opt.*, **15**, 055002.
72. Yeh, A. T., Choi, B., Nelson, J. S., and Tromberg, B. J. (2003) Reversible dissociation of collagen in tissues, *J. Invest. Dermatol.*, **121**, 1332-1335.
73. Berezin, K. V., Dvoretski, K. N., Chernavina, M. L., Likhter, A. M., Smirnov, V. V., Shagautdinova, I. T., Antonova, E. M., Stepanovich, E. Y., Dzhalmuhambetova,

E. A., and Tuchin, V. V. (2018) Molecular modeling of immersion optical clearing of biological tissues, *J. Mol. Model.*, **24**, 45.
74. Askar'yan, G. A. (1982). Enhancement of transmission of laser and other radiation by soft turbid physical and biological media, *Soviet J. Quantum Electron.*, **12**, 877-880.
75. Chan, E. K., Sorg, B., Protsenko, D., O'Neil, M., Motamedi, M., and Welch, A. J. (1996) Effects of compression on soft tissue optical properties, *IEEE J. Sel. Top. Quantum Electron.*, **2**, 943-950.
76. Ding, H. F., Lu, J. Q., Wooden, W. A., Kragel, P. J., and Hu, X. H. (2006) Refractive indices of human skin tissues at eight wavelengths and estimated dispersion relations between 300 and 1600 nm, *Phys. Med. Biol.*, **51**, 1479-1489.
77. Hoyt, L. F. (1934) New table of the refractive index of pure glycerol at 20°C, *Ind. Eng. Chem.*, **26**, 329-332.
78. Genina, E. A., Bashkatov, A. N., Kochubey, V. I., and Tuchin, V. V. (2005) Optical clearing of human dura mater, *Opt. Spectrosc.*, **98**, 470-476.
79. Vargas, O., Chan, E. K., Barton, J. K., Rylander, H. G., and Welch, A. J. (1999) Use of an agent to reduce scattering in skin, *Laser Surg. Med.*, **24**, 133-141.
80. Bashkatov, A. N., Genina, E. A., Sinichkin, Y. P., Kochubey, V. I., Lakodina, N. A., and Tuchin, V. V. (2003) Glucose and mannitol diffusion in human dura mater, *Biophys. J.*, **85**, 3310-3318.
81. Bashkatov, A. N., Genina, E. A., and Tuchin, V. V. (2009) in *Handbook of Optical Sensing of Glucose in Biological Fluids and Tissues* (Tuchin, V. V., ed.), CRC Press, Boca Raton.
82. Vargas, G., Barton, J. K., and Welch, A. J. (2008) Use of hyperosmotic chemical agent to improve the laser treatment of cutaneous vascular lesions, *J. Biomed. Opt.*, **13**, 021114.
83. Sun, R. W., Tuchin, V. V., Zharov, V. P., Galanzha, E. I., and Richter, G. T. (2018). Current status, pitfalls and future directions in the diagnosis and therapy of lymphatic malformation, *J. Biophotonics*, **11**, e201700124.
84. Genina, E. A., Bashkatov, A. N., Sinichkin, Yu. P., and Tuchin, V. V. (2006) Optical clearing of eye sclera *in vivo* caused by glucose, *Quantum Electron.*, **36**, 1119-1124.
85. Bashkatov, A. N., Korolevich, A. N., Tuchin, V. V., Sinichkin, Yu. P., Genina, E. A., Stolnitz, M. M., Dubina, N. S., Vecherinski, S. I., and Belsley, M. S. (2006) *In vivo* investigation of human skin optical clearing and blood microcirculation under the action of glucose solution, *Asian J. Phys.*, **15**, 1-14.
86. Galanzha, E. I., Tuchin, V. V., Solovieva, A. V., Stepanova, T. V., Luo, Q., and Cheng, H. (2003) Skin backreflectance and microvascular system functioning at the action of osmotic agents, *J. Phys. D: Appl. Phys.*, **36**, 1739-1746.
87. Zhu, D., Zhang, J., Cui, H., Mao, Z., Li, P., and Luo, Q. (2008) Short-term and long-term effects of optical clearing agents on blood vessels in chick chorioallantoic membrane, *J. Biomed. Opt.*, **13**, 021106.
88. Zhu, Z. G., Wu, G. Y., Wei, H. J., Yang, H. Q., He, Y. H., Xie, S. S., Zhao, Q. L., and Guo, X. (2012) Investigation of the permeability and optical clearing ability of different analytes in human normal and cancerous breast tissues by spectral domain OCT, *J. Biophotonics*, **5**, 536-543.
89. Genina, E. A., Bashkatov, A. N., Korobko, A. A., Zubkova, E. A., Tuchin, V. V., Yaroslavsky, I., and Altshuler, G. B. (2008) Optical clearing of human skin: comparative study of permeability and dehydration of intact and photothermally perforated skin, *J. Biomed. Opt.*, **13**, 021102.
90. Genina, E. A., Bashkatov, A. N., Sinichkin, Yu. P., and Tuchin, V. V. (2010) Optical clearing of skin under action of glycerol: *ex vivo* and *in vivo* investigations, *Opt. Spectrosc.*, **109**, 225-231.
91. Choi, B., Tsu, L., Chen, E., Ishak, T. S., Iskandar, S. M., Chess, S., and Nelson, J. S. (2005) Determination of chemical agent optical clearing potential using *in vitro* human skin, *Laser Surg. Med.*, **36**, 72-75.
92. Khan, M. H., Choi, B., Chess, S., Kelly, K. M., McCullough, J., and Nelson, J. S. (2004) Optical clearing of *in vivo* human skin: implications for light-based diagnostic imaging and therapeutics, *Laser Surg. Med.*, **34**, 83-85.
93. Mao, Z., Zhu, D., Hu, Y., Wen, X., and Han, Z. (2008) Influence of alcohols on the optical clearing effect of skin *in vitro*, *J. Biomed. Opt.*, **13**, 021104.
94. Proskurin, S. G., and Meglinski, I. V. (2007) Optical coherence tomography imaging depth enhancement by superficial skin optical clearing, *Laser Phys. Lett.*, **4**, 824-826.
95. Genina, E. A., Bashkatov, A. N., and Tuchin, V. V. (2008) Optical clearing of cranial bone, *Adv. Opt. Technol.*, **2008**, 1-8.
96. Ghosn, M. G., Tuchin, V. V., and Larin, K. V. (2006) Depth-resolved monitoring of glucose diffusion in tissues by using optical coherence tomography, *Opt. Lett.*, **31**, 2314-2316.
97. Wang, J., Ma, N., Shi, R., Zhang, Y., Yu, T. T., and Zhu, D. (2014) Sugar-induced skin optical clearing: from molecular dynamics simulation to experimental demonstration, *IEEE J. Sel. Top. Quant. Electron.*, **20**, 7101007.
98. Bashkatov, A. N., Genina, E. A., Sinichkin, Yu. P., Kochubei, I. V., Lakodina, N. A., and Tuchin, V. V. (2003) Determination of glucose diffusion coefficient in human eye sclera, *Biophysics*, **48**, 309-313.
99. Tuchina, D. K., Timoshina, P. A., Tuchin, V. V., Bashkatov, A. N., and Genina, E. A. (2019). Kinetics of rat skin optical clearing at topical application of 40% glucose: *ex vivo* and *in vivo* studies, *IEEE J. Sel. Top. Quant. Electron.*, **25**, 1-8.
100. Jiang, J. Y., and Wang, R. K. K. (2004) Comparing the synergistic effects of oleic acid and dimethyl sulfoxide as vehicles for optical clearing of skin tissue *in vitro*, *Phys. Med. Biol.*, **49**, 5283-5294.
101. Xu, X. Q., and Wang, R. K. K. (2004) Synergistic effect of hyperosmotic agents of dimethyl sulfoxide and glycerol on optical clearing of gastric tissue studied with near infrared spectroscopy, *Phys. Med. Biol.*, **49**, 457-468.
102. Ding, Y. M., Wang, J., Fan, Z. C., Wei, D., Shi, R., Luo, Q. M., Zhu, D., and Wei, X. B. (2013) Signal and depth enhancement for *in vivo* flow cytometer measurement of ear skin by optical clearing agents, *Biomed. Opt. Express*, **4**, 2518-2526.
103. Shi, R., Guo, L., Zhang, C., Feng, W., Li, P., Ding, Z., and Zhu, D. (2016) A useful way to develop effective *in vivo* skin optical clearing agents, *J. Biophotonics*, **10**, 887-895.

104. Deng, Z., Jing, L., Wu, N., Jiang, X., Ren, Q., and Li, C. (2014) Viscous optical clearing agent for *in vivo* optical imaging, *J. Biomed. Opt.*, **19**, 76019.
105. Guo, L., Shi, R., Zhang, C., Zhu, D., Ding, Z., and Li, P. (2016) Optical coherence tomography angiography offers comprehensive evaluation of skin optical clearing *in vivo* by quantifying optical properties and blood flow imaging simultaneously, *J. Biomed. Opt.*, **21**, 081202.
106. Jin, X., Deng, Z., Wang, J., Ye, Q., Mei, J., Zhou, W., Zhang, C., and Tian, J. (2016) Study of the inhibition effect of thiazone on muscle optical clearing, *J. Biomed. Opt.*, **21**, 105004.
107. Wang, J., Shi, R., and Zhu, D. (2012) Switchable skin window induced by optical clearing method for dermal blood flow imaging, *J. Biomed. Opt.*, **18**, 061209.
108. Zhong, H. Q., Guo, Z. Y., Wei, H. J., Guo, L., Wang, C. X., He, Y. H., Xiong, H. L., and Liu, S. H. (2010) Synergistic effect of ultrasound and thiazone-PEG 400 on human skin optical clearing *in vivo*, *Photochem. Photobiol.*, **86**, 732-737.
109. Shi, R., Chen, M., Tuchin, V. V., and Zhu, D. (2015) Accessing to arteriovenous blood flow dynamics response using combined laser speckle contrast imaging and skin optical clearing, *Biomed. Opt. Express*, **6**, 1977-1989.
110. Plotnikov, S., Juneja, V., Isaacson, A. B., Mohler, W. A., and Campagnola, P. J. (2006) Optical clearing for improved contrast in second harmonic generation imaging of skeletal muscle, *Biophys. J.*, **90**, 328-339.
111. Wen, X., Jacques, S. L., Tuchin, V. V., and Zhu, D. (2012) Enhanced optical clearing of skin *in vivo* and optical coherence tomography in-depth imaging, *J. Biomed. Opt.*, **17**, 066022.
112. Vargas, G., Readinger, A., Dozier, S. S., and Welch, A. J. (2003) Morphological changes in blood vessels produced by hyperosmotic agents and measured by optical coherence tomography, *Photochem. Photobiol.*, **77**, 541-549.
113. Larina, I. V., Carbajal, E. F., Tuchin, V. V., Dickinson, M. E., and Larin, K. V. (2008) Enhanced OCT imaging of embryonic tissue with optical clearing, *Laser Phys. Lett.*, **5**, 476-479.
114. Sudheendran, N., Mohamed, M., Ghosn, M. G., Tuchin, V. V., and Larin, K. V. (2010) Assessment of tissue optical clearing as a function of glucose concentration using optical coherence tomography, *J. Innov. Opt. Heal. Sci.*, **3**, 169-176.
115. Xu, X. Q., and Zhu, Q. H. (2007) Evaluation of skin optical clearing enhancement with Azone as a penetration enhancer, *Opt. Commun.*, **279**, 223-228.
116. Zhi, Z. W., Han, Z. Z., Luo, Q. M., and Zhu, D. (2009) Improve optical clearing of skin *in vitro* with propylene glycol as a penetration enhancer, *J. Innov. Opt. Heal. Sci.*, **2**, 269-278.
117. Caspers, P. J., Williams, A. C., Carter, E. A., Edwards, H. G., Barry, B. W., Bruining, H. A., and Puppels, G. J. (2002) Monitoring the penetration enhancer dimethyl sulfoxide in human stratum corneum *in vivo* by confocal Raman spectroscopy, *Pharm. Res.*, **19**, 1577-1580.
118. Notman, R., den Otter, W. K., Noro, M. G., Briels, W. J., and Anwar, J. (2007) The permeability enhancing mechanism of DMSO in ceramide bilayers simulated by molecular dynamics, *Biophys. J.*, **93**, 2056-2068.
119. Vejnovic, I., Simmler, L., and Betz, G. (2010) Investigation of different formulations for drug delivery through the nail plate, *Int. J. Pharm.*, **386**, 185-194.
120. Kuriharabergstrom, T., Knutson, K., Denoble, L. J., and Goates, C. Y. (1990) Percutaneous absorption enhancement of an ionic molecule by ethanol–water systems in human skin, *Pharm. Res.*, **7**, 762-766.
121. Timoshina, P. A., Zinchenko, E. M., Tuchina, D. K., Sagatova, M. M., Semyachkina-Glushkovskaya, O. V., and Tuchin, V. V. (2017) Laser speckle contrast imaging of cerebral blood flow of newborn mice at optical clearing, *Proc. SPIE*, **10336**, 1033610.
122. Liu, P., Huang, Y., Guo, Z., Wang, J., Zhuang, Z., and Liu, S. (2013) Discrimination of dimethyl sulphoxide diffusion coefficient in the process of optical clearing by confocal micro-Raman spectroscopy, *J. Biomed. Opt.*, **18**, 20507.
123. Samatham, R., Phillips, K. G., and Jacques, S. L. (2010) Assessment of optical clearing agents using reflectance-mode confocal scanning laser microscopy, *J. Innov. Opt. Heal. Sci.*, **3**, 183-188.
124. Millon, S. R., Roldan-Perez, K. M., Riching, K. M., Palmer, G. M., and Ramanujam, N. (2006) Effect of optical clearing agents on the *in vivo* optical properties of squamous epithelial tissue, *Laser Surg. Med.*, **38**, 920-927.
125. Vargas, G., Chan, K. F., Thomsen, S. L., and Welch, A. J. (2001) Use of osmotically active agents to alter optical properties of tissue: effects on the detected fluorescence signal measured through skin, *Laser Surg. Med.*, **29**, 213-220.
126. Weigmann, H. J., Lademann, J., Schanzer, S., Lindemann, U., von Pelchrzim, R., Schaefer, H., Sterry, W., and Shah, V. (2001) Correlation of the local distribution of topically applied substances inside the stratum corneum determined by tape-stripping to differences in bioavailability, *Skin Pharmacol. Appl. Skin Physiol.*, **14** (Suppl. 1), 98-102.
127. Stumpp, O., Chen, B., and Welch, A. J. (2006) Using sandpaper for noninvasive transepidermal optical skin clearing agent delivery, *J. Biomed. Opt.*, **11**, 041118.
128. Lee, W. R., Tsai, R. Y., Fang, C. L., Liu, C. J., Hu, C. H., and Fang, J. Y. (2006) Microdermabrasion as a novel tool to enhance drug delivery via the skin: an animal study, *Dermatol. Surg.*, **32**, 1013-1022.
129. Tuchin, V. V., Altshuler, G. B., Gavrilova, A. A., Pravdin, A. B., Tabatadze, D., Childs, J., and Yaroslavsky, I. V. (2006) Optical clearing of skin using flashlamp-induced enhancement of epidermal permeability, *Laser Surg. Med.*, **38**, 824-836.
130. Stumpp, O. F., Welch, A. J., Milner, T. E., and Neev, J. (2005) Enhancement of transepidermal skin clearing agent delivery using a 980 nm diode laser, *Laser Surg. Med.*, **37**, 278-285.
131. Liu, C., Zhi, Z., Tuchin, V. V., and Zhu, D. (2009) Combined laser and glycerol enhancing skin optical clearing, *Proc. SPIE*, **7186**, 71860D.
132. Nugroho, A. K., Li, G. L., Danhof, M., and Bouwstra, J. A. (2004) Transdermal iontophoresis of rotigotine across human stratum corneum *in vitro*: influence of pH and NaCl concentration, *Pharm. Res.*, **21**, 844-850.
133. Tezel, A., and Mitragotri, S. (2003) Interactions of inertial cavitation bubbles with stratum corneum lipid bilayers

during low-frequency sonophoresis, *Biophys. J.*, **85**, 3502-3512.
134. Konig, K. (2008) Clinical multiphoton tomography, *J. Biophotonics*, **1**, 13-23.
135. Tseng, S. J., Lee, Y. H., Chen, Z. H., Lin, H. H., Lin, C. Y., and Tang, S. C. (2009) Integration of optical clearing and optical sectioning microscopy for three-dimensional imaging of natural biomaterial scaffolds in thin sections, *J. Biomed. Opt.*, **14**, 044004.
136. Chiang, Ann-Shyn, Aqueous tissue clearing solution, US Patent No. 6,472,216, October 29, 2002.
137. Cicchi, R., Sestini, S., De Giorgi, V., Massi, D., Lotti, T., and Pavone, F. S. (2008) Nonlinear laser imaging of skin lesions, *J. Biophotonics*, **1**, 62-73.
138. Klemp, M., Meinke, M. C., Weinigel, M., Rowert-Huber, H. J., Konig, K., Ulrich, M., Lademann, J., and Darvin, M. E. (2016) Comparison of morphologic criteria for actinic keratosis and squamous cell carcinoma using *in vivo* multiphoton tomography, *Exp. Dermatol.*, **25**, 218-222.
139. Hovhannisyan, V. A., Hu, P. S., Chen, S. J., Kim, C. S., and Dong, C. Y. (2013) Elucidation of the mechanisms of optical clearing in collagen tissue with multiphoton imaging, *J. Biomed. Opt.*, **18**, 046004.
140. Migacheva, E. V., Pravdin, A. B., and Tuchin, V. V. (2010) Alterations in autofluorescence signal from rat skin *ex vivo* under optical immersion clearing, *J. Innov. Opt. Heal. Sci.*, **3**, 147-152.
141. Kong, K., Kendall, C., Stone, N., and Notingher, I. (2015) Raman spectroscopy for medical diagnostics – from *in vitro* biofluid assays to *in vivo* cancer detection, *Adv. Drug Deliver Rev.*, **89**, 121-134.
142. Krafft, C., Schmitt, M., Schie, I. W., Cialla-May, D., Matthaus, C., Bocklitz, T., and Popp, J. (2017) Label-free molecular imaging of biological cells and tissues by linear and nonlinear Raman spectroscopic approaches, *Angew. Chem. Int. Edit.*, **56**, 4392-4430.
143. Jermyn, M., Desroches, J., Aubertin, K., St-Arnaud, K., Madore, W. J., De Montigny, E., Guiot, M. C., Trudel, D., Wilson, B. C., Petrecca, K., and Leblond, F. (2016) A review of Raman spectroscopy advances with an emphasis on clinical translation challenges in oncology, *Phys. Med. Biol.*, **61**, R370-R400.
144. Binder, L., SheikhRezaei, S., Baierl, A., Gruber, L., Wolzt, M., and Valenta, C. (2017) Confocal Raman spectroscopy: *in vivo* measurement of physiological skin parameters – a pilot study, *J. Dermatol. Sci.*, **88**, 280-288.
145. Choe, C., Schleusener, J., Lademann, J., and Darvin, M. E. (2017) Age related depth profiles of human *stratum corneum* barrier-related molecular parameters by confocal Raman microscopy *in vivo*, *Mech. Ageing Dev.*, **172**, 6-12.
146. Darvin, M. E., Gersonde, I., Ey, S., Brandt, N. N., Albrecht, H., Gonchukov, S. A., Sterry, W., and Lademann, J. (2004) Noninvasive detection of beta-carotene and lycopene in human skin using Raman spectroscopy, *Laser Phys.*, **14**, 231-233.
147. Richters, R. J., Falcone, D., Uzunbajakava, N. E., Varghese, B., Caspers, P. J., Puppels, G. J., van Erp, P. E., and van de Kerkhof, P. C. (2017) Sensitive skin: assessment of the skin barrier using confocal Raman microspectroscopy, *Skin Pharmac. Physiol.*, **30**, 1-12.
148. Choe, C., Lademann, J., and Darvin, M. E. (2015) Analysis of human and porcine skin *in vivo*/*ex vivo* for penetration of selected oils by confocal Raman microscopy, *Skin Pharmac. Physiol.*, **28**, 318-330.
149. Binder, L., Kulovits, E. M., Petz, R., Ruthofer, J., Baurecht, D., Klang, V., and Valenta, C. (2018) Penetration monitoring of drugs and additives by ATR-FTIR spectroscopy/tape stripping and confocal Raman spectroscopy – a comparative study, *Eur. J. Pharm. Biopharm.*, **130**, 214-223.
150. Mujica Ascencio, S., Choe, C., Meinke, M. C., Muller, R. H., Maksimov, G. V., Wigger-Alberti, W., Lademann, J., and Darvin, M. E. (2016) Confocal Raman microscopy and multivariate statistical analysis for determination of different penetration abilities of caffeine and propylene glycol applied simultaneously in a mixture on porcine skin *ex vivo*, *Eur. J. Pharm. Biopharm.*, **104**, 51-58.
151. Enejder, A. M. K., Scecina, T. G., Oh, J., Hunter, M., Shih, W. C., Sasic, S., Horowitz, G. L., and Feld, M. S. (2005) Raman spectroscopy for noninvasive glucose measurements, *J. Biomed. Opt.*, **10**, 031114.
152. McNichols, R. J., and Cote, G. L. (2000) Optical glucose sensing in biological fluids: an overview, *J. Biomed. Opt.*, **5**, 5-16.
153. Quatela, A., Miloudi, L., Tfayli, A., and Baillet-Guffroy, A. (2016) *In vivo* Raman microspectroscopy: intra- and intersubject variability of *stratum corneum* spectral markers, *Skin Pharmacol. Physiol.*, **29**, 102-109.
154. Zimmerley, M., McClure, R. A., Choi, B., and Potma, E. O. (2009) Following dimethyl sulfoxide skin optical clearing dynamics with quantitative nonlinear multimodal microscopy, *Appl. Optics*, **48**, D79-D87.
155. Huang, D., Zhang, W., Zhong, H., Xiong, H., Guo, X., and Guo, Z. (2012) Optical clearing of porcine skin tissue *in vitro* studied by Raman microspectroscopy, *J. Biomed. Opt.*, **17**, 015004.
156. Kim, S., Byun, K. M., and Lee, S. Y. (2017) Influence of water content on Raman spectroscopy characterization of skin sample, *Biomed. Opt. Express*, **8**, 1130-1138.
157. Choe, C., Schleusener, J., Lademann, J., and Darvin, M. E. (2018) Human skin *in vivo* has a higher skin barrier function than porcine skin *ex vivo* – comprehensive Raman microscopic study of the *stratum corneum*, *J. Biophotonics*, **11**, e201700355.
158. Hokr, B. H., and Yakovlev, V. V. (2013) Raman signal enhancement via elastic light scattering, *Opt. Express*, **21**, 11757-11762.
159. Matousek, P. (2007) Raman signal enhancement in deep spectroscopy of turbid media, *Appl. Spectrosc.*, **61**, 845-854.
160. Oelkrug, D., Boldrini, B., and Rebner, K. (2017) Comparative Raman study of transparent and turbid materials: models and experiments in the remote sensing mode, *Anal. Bioanal. Chem.*, **409**, 673-681.
161. Zhu, Y., Choe, C. S., Ahlberg, S., Meinke, M. C., Alexiev, U., Lademann, J., and Darvin, M. E. (2015) Penetration of silver nanoparticles into porcine skin *ex vivo* using fluorescence lifetime imaging microscopy, Raman microscopy, and surface-enhanced Raman scattering microscopy, *J. Biomed. Opt.*, **20**, 051006.
162. Wang, Y., Ji, W., Yu, Z., Li, R., Wang, X., Song, W., Ruan, W. D., Zhao, B., and Ozaki, Y. (2014) Contribution of

hydrogen bonding to charge-transfer induced surface-enhanced Raman scattering of an intermolecular system comprising *p*-aminothiophenol and benzoic acid, *Phys. Chem. Chem. Phys.*, **16**, 3153-3161.

163. Yamamoto, Y. S., Ishikawa, M., Ozaki, Y., and Itoh, T. (2014) Fundamental studies on enhancement and blinking mechanism of surface-enhanced Raman scattering (SERS) and basic applications of SERS biological sensing, *Front. Phys. (Beijing)*, **9**, 31-46.
164. Zhang, Y. F., Li, D. Q., Zhou, X. Y., Gao, X. H., Zhao, S. Y., and Li, C. (2016) Enhancing sensitivity of SERRS nanoprobes by modifying heptamethine cyanine-based reporter molecules, *J. Innov. Opt. Heal. Sci.*, **9**, 1642005.
165. Ozaki, Y., Kneipp, K., and Aroca, R. (2014) *Frontiers of Surface-Enhanced Raman Scattering: Single Nanoparticles and Single Cells*, John Wiley & Sons, Chichester.
166. Zhang, Y., Liu, H., Tang, J., Li, Z., Zhou, X., Zhang, R., Chen, L., Mao, Y., and Li, C. (2017) Noninvasively imaging subcutaneous tumor xenograft by a handheld Raman detector, with the assistance of an optical clearing agent, *ACS Appl. Mater. Interfaces*, **9**, 17769-17776.
167. Darvin, M. E., Schleusener, J., Parenz, F., Seidel, O., Krafft, C., Popp, J., and Lademann, J. (2018) Confocal Raman microscopy combined with optical clearing for identification of inks in multicolored tattooed skin *in vivo*, *Analyst*, **143**, 4990-4999.
168. Choe, C., Lademann, J., and Darvin, M. E. (2016) Depth profiles of hydrogen bound water molecule types and their relation to lipid and protein interaction in the human *stratum corneum in vivo*, *Analyst*, **141**, 6329-6337.
169. Choe, C., Schleusener, J., Lademann, J., and Darvin, M. E. (2017) Keratin–water–NMF interaction as a three layer model in the human *stratum corneum* using *in vivo* confocal Raman microscopy, *Sci. Rep.*, **7**, 15900.
170. Sdobnov, A. Y., Darvin, M. E., Schleusener, J., Lademann, J., and Tuchin, V. V. (2018) Hydrogen bound water profiles in the skin influenced by optical clearing molecular agents – quantitative analysis using confocal Raman microscopy, *J. Biophotonics*, e201800283; doi: 10.1002/jbio.201800283.
171. Nakagawa, N., Matsumoto, M., and Sakai, S. (2010) *In vivo* measurement of the water content in the dermis by confocal Raman spectroscopy, *Skin Res. Technol.*, **16**, 137-141.